Modal interferometer based on tapering single-mode-multimode-single-mode fiber structure by hydrogen flame

Ying Zhang (张 英), Weiwen Zou (邹卫文)*, Xinwan Li (李新碗), Jingwei Mao (毛经纬), Wenning Jiang (姜文宁), and Jianping Chen (陈建平)

The State Key Laboratory of Advanced Optical Communication Systems and Networks, Shanghai Jiao Tong University, Shanghai 200240, China

**Corresponding author: wzou@sjtu.edu.cn*

Received October 12, 2011; accepted January 18, 2012; posted online April 12, 2012

A modal interferometer is experimentally demonstrated based on tapering a single-mode-multimode-single-mode (SMS) fiber structure heated by hydrogen flame. The interference fringe begins to form when tapering length is 19.8 mm, and becomes regular and clear when the tapering length is longer and the tapered waist diameter is smaller. Annealing process is undertaken to achieve a high extension ratio of approximately 17 dB with free spectral range of 1.5 nm when the tapering length is 33 mm and the tapered waist diameter is approximately 5 μm. The temperature and axial strain dependences of the tapered SMS structure are characterized, and the measured temperature and strain coefficients are +7 pm/°C and –9.536 pm/$\mu\varepsilon$, respectively.

OCIS codes: 060.2340, 130.3990, 230.4000.
doi: 10.3788/COL201210.070609.

Optical fiber modal interferometers are built based on the coupling of multiple propagating modes, which have many potential applications in detecting temperature, strain, external refractive index (RI), and so on. Thus far, several methods have been demonstrated to configure optical fiber modal interferometers by core-offsetting[1,2], cascading taper structure[3–5], and configuring single-mode-multimode-single-mode (SMS) fiber structures[6–8]. Core offsetting requires precise manipulation, whereas cascading taper structure has the drawback of complex fabrication. Comparably, a SMS fiber structure offers advantages such as low cost, easy fabrication, and feasible tailoring of the interfering transmission spectrum[9]. In order to further utilize the cladding modes in the multimode interference, the multimode fiber (MMF) in the middle of the SMS structure is tapered by chemically etching with hydrofluoric acid[10] or CO_2 laser beam heating[11]. A detailed theoretical study of the tapered SMS structure was demonstrated in Ref. [12]. Tapered SMS[10,11] provides high sensitivity to the external refractive index, showing great potential application in biochemical sensing. Its resolution is determined by the interference fringes; therefore obtaining high-resolution detection using an abrupt taper structure[11] is difficult due to interference fringe irregularity.

In this letter, we demonstrate a modal interferometer based on tapering a SMS structure heated by hydrogen flame, which is more easily fabricated and has more regular interference fringes than the structure in Ref. [11]. The taper waist diameter achieved can be as small as ~5 μm. We experimentally realized a regular interference fringe with the free spectral range (FSR) of 1.5 nm after the annealing process when the taper waist diameter achieved was as small as ~5 μm. The temperature and strain dependences of the 1.5-nm FSR modal interferometer were also studied. The interference fringe red-shifted with temperature (+7 pm/°C), but blue-shifted with strain (–9.536 pm/$\mu\varepsilon$). This structure showed better temperature stability and higher strain sensitivity than the SMS structure without tapering.

The SMS structure was configured by striping, cleaving and splicing a 50-mm MMF with two pieces of SMF. MMF had a step-index profile with core/cladding diameter of 105 μm/125 μm. As schematically shown in Fig. 1, the SMS structure was mounted onto two translation stages that can be automatically driven by two piezoelectric actuators. A hydrogen flame of 6 mm in width was used to heat the center of the SMS structure, which was then horizontally drawn by the two piezoelectric actuators with a speed of 0.16 mm/s[13,14]. To ensure uniform heating, the hydrogen flame was also controlled by a piezoelectric actuator that can be alternatively switched on or off.

For *in situ* measurement of the transmission spectrum during the tapering process, an amplification of spontaneous emission (ASE) light source with a wavelength range from 1 510 to 1 590 nm and an optical spectrum analyzer (OSA) (AQ6370C Yokogawa, Japan) with an optical resolution of 0.02 nm and sensitivity of 0.01 nm were used.

The measured transmission spectra of the tapered SMS

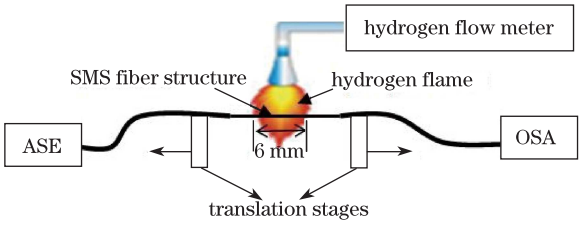

Fig. 1. Experimental setup for tapering SMS structure and *in situ* measurement of the transmission spectrum.

structure with different tapering lengths are shown in Fig. 2. Figure 2(a) shows that the interference fringe began to be formed when tapering length was L=19.8 mm and the diameter of the uniform waist region was D =∼25 μm. Under this situation, too many higher-order modes interference made the interference fringes irregular. When the tapering length L was increased from 26.4 to 33 mm and the taper waist D decreased from ∼15 to ∼5 μm, the interference fringes become regular, as illustrated in Figs. 2(b) and (c). FSRs were estimated to be 4 and 1.5 nm, respectively, because higher-order modes were filtered as the taper waist diameter decreased and more energy of fundamental mode was coupled to lower-order modes.

We should note that all the three spectra were recorded when the hydrogen flame was moved away. The measured interference fringes were quite noisy, with high transition loss and low extinction ratio of ∼10 dB, likely due to the residual stress stored in the tapered structure during the drawing process under a high-temperature hydrogen flame. Due to the elasto-optic effect, the residual stress modified the refractive index distribution and introduced the interference ripples (see Fig. 2(c)). In order to release the residual stress, the tapered structure with a uniform waist of D =∼5 μm was annealed using a temperature controller. After annealing for 2 h, the interference fringe in Fig. 2(c) was measured again. The result depicted in Fig. 2(d) shows a clean interference fringe with high extinction ratio of ∼17 dB and much lower transmission loss. The insertion loss of the interferometer after the annealing process was 2 dB.

The interference fringe occurring in the tapered SMS fiber structure can be explained by the theory of the modal interferometer. Figure 3(a) depicts the overall view of the tapered SMS structure comprising two MMF transition regions (left, first; right, second) and a smooth waist region. Figure 3(b) shows an example of the SEM image of the smooth waist region (D =∼5 μm). The fundamental mode LP_{01} passed through the interface between the left SMF section and the first transition region of the tapered MMF, thereby generating multiple modes. For nonadiabatic taper angles formed in the middle multimode fiber, high-efficiency coupling among the fundamental LP_{01} and the high LP_{0m} cladding modes takes place[15]. In the smooth-waist region, higher-order LP_{0m} modes suffered greater loss, whereas the lower-order LP_{0m} modes suffered lower loss during

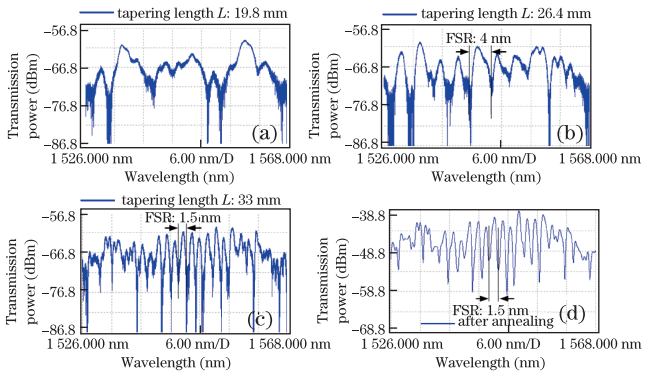

Fig. 2. Transmission spectra of the tapered SMS structure (a–c) with different tapering lengths and (d) after annealing.

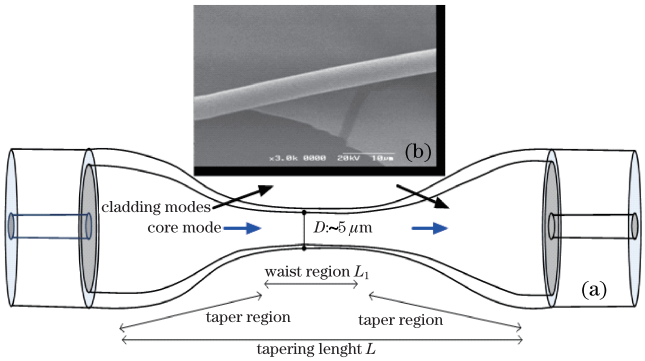

Fig. 3. (a) Overview of the tapered SMS structure; (b) SEM image of the smooth waist region (D =∼5 μm).

propagation. Consequently, the interference between LP_{01} and lower-order LP_{0m} became more dominant, as comparatively shown in Figs. 2(a) and (b). When the beam further propagating in the smooth-waist region and leaving the interface between the second SMF and the second transition region, a Mach-Zehnder-like interferometer was formed, because few modes have different effective refractive indices, although they share the same physical arm (the tapered smooth-waist region).

FSR of the interference fringes is approximately dependent on the length of the smooth waist region (L_1) as[16]

$$\mathrm{FSR} \approx \frac{\lambda^2}{\Delta n_{\mathrm{eff}}^{m} L_1}, \tag{1}$$

where λ is the light wavelength in vacuum, and $\Delta n_{\mathrm{eff}}^{m}$ is the effective refractive index difference between the fundamental core mode and the mth-order higher modes. According to Eq (1), FSR decreased as the length L_1 increased, which is in agreement with the experimental results shown in Figs. 2(b) and (c).

Comparing the reported modal interferometers implemented by core-offsetting[1,2], cascading taper structure[3−5], and splicing a piece of photonic crystal fiber (PCF) with two SMFs[17], the one demonstrated here has advantages of long-length interference range in the smooth waist region, easy fabrication, and good repeatability. Less modes existed in the tapered multimode fiber because the core/ cladding diameter was sharply shrunk from 105 μm/125 μm to 4.2 μm/5 μm. Thus, the intensity of modes involved in forming interference fringes became much stronger and much closer to one another, leading to more regular and clearer interference patterns (see Figs. 2(c) and (d)).

Temperature and axial strain dependences of the modal interferometer based on the tapered SMS structure were also studied. As described in Ref. [18], the temperature dependence of the SMS structure without tapering is dominantly relative to thermal expansion of the packaging materials. In order to measure temperature dependence, one SMS structure without any tapering as reference and the other SMS structure with 33-mm tapering length were placed together into a temperature controller under the same packaging conditions. The temperature was increased to 80 °C from 20 °C at a rate of 5°C each time. Figure 4(a) depicts the measured transmission spectra with tapering 33 mm, both shifting towards the greater wavelength (red-shifting) with the

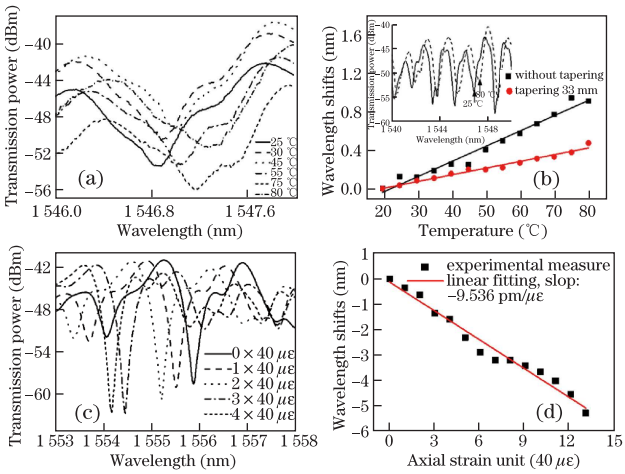

Fig. 4. (Color online) Measured transmission spectra at (a) different temperatures or under (c) different strains; the characterized wavelength shift as functions of (b) temperature and (d) strain.

increased temperature. The red-shifted wavelength at the dip of the spectrum as a function of temperature is illustrated in Fig. 4(b). After least-squares linear fitting to the experimental data, the temperature coefficient was evaluated to be +15.93 pm/°C for the SMS structure without tapering and +7 pm/°C for the tapered one. In comparison, the temperature coefficient of the tapered SMS structure was two times smaller, indicating better temperature stability.

In order to characterize strain dependence, the tapered SMS structure with 33-mm tapering length was fixed onto two additional transaction stages so that the axial strain could be applied in unit of 40 $\mu\varepsilon$ (=0.0033 mm/83 mm). Figure 4(c) shows the measured transmission spectra under different strains. The interference dip shifted towards the smaller wavelength (blue-shifted) with respect to the applied strain. The wavelength shift had good linear dependence on strain (see Fig. 4(d)). The strain coefficient was deduced as –9.536 pm/$\mu\varepsilon$ by the least-squares linear fitting. For the SMS structure without tapering, the spectrum blue-shifts with a rate of ~2.5 pm/$\mu\varepsilon$[19]. Obviously, the interferometer demonstrated in this study was more sensitive than the SMS structure without tapering, and much more sensitive than a standard fiber Bragg grating (FBG)-based strain sensor (~1.22 pm/$\mu\varepsilon$).

In conclusion, we experimentally demonstrate a modal interferometer based on tapering a SMS structure by hydrogen-flame heating. This structure can be easily configured with a thin waist diameter as small as ~5 μm and a long-length smooth waist region. The thin waist acts as a mode filter to minimize mode interference. Appropriate FSR of the interference fringe can be obtained by controlling the tapering length. Annealing is necessary to achieve clean interference fringe. A modal interferometer with FSR of 1.5 nm is successfully obtained. Its temperature and strain dependences are studied. The measured results show that it has better performance in temperature stability (+7 pm/°C) and axial strain sensing ability (–9.536 pm/$\mu\varepsilon$) than the SMS structure without tapering. The proposed modal interferometer may have potential applications in tunable comb filters, fiber lasers, and fiber sensors.

This work was supported in part by the National "973" Program of China (No. 2011CB301700), the National Natural Science Foundation of China (Nos. 61007052, 61071011, 61107041, 61127016), the International Cooperation Project from the Ministry of Science and Technology of China (No. 2011FDA11780), the STCSM Project (Nos. 09JC1408100, 10DJ1400402), the "SMC Young Star" Scientist Program of Shanghai Jiao Tong University, and the National Key Lab Projects (No. GKZD030021).

References

1. Z. Tian, S. S.-H. Yam, and H.-P. Loock, IEEE Photon. Technol. Lett. **20,** 1387 (2008).
2. B. Dong, D. P. Zhou, L. Wei, W-K. Liu, and J. W. Y. Lit, Opt. Express **16,** 19291 (2008).
3. T. Wei, X. Lan, and H. Xiao, IEEE Photon. Technol. Lett. **21,** 669 (2009).
4. Z. Tian, S. S-H. Yam, and H-P. Loock, Opt. Lett. **33,** 1105 (2008).
5. Z-Z. Feng, Y-H. Hsieh, and N-K. Chen, IEEE Photon. Technol. Lett. **23,** 438 (2011).
6. A. Mehta, W. Mohammed, and E. G. Johnson, IEEE Photon. Technol. Lett. **15,** 1129 (2003).
7. E. Li, IEEE Photon. Technol. Lett. **19,** 1266 (2007).
8. E. B. Li, X. L. Wang, and C. Zhang, Appl. Phys. Lett. **89,** 091119 (2006).
9. Q. Wang, G. Farrell, and W. Yan, J. Lightwave Technol. **26,** 512 (2008).
10. Q. Wu, Y. Semenova, P. Wang, and G. Farrell, Opt. Express **19,** 7937 (2011).
11. P. Wang, G. Brambilla, M. Ding, Y. Semenova, Q. Wu, and G. Farrell, Opt. Lett. **36,** 2233 (2011).
12. P. Wang, G. Brambilla, M. Ding, Y. Semenova, Q. Wu, and G. Farrell, J. Opt. Soc. Am. B **28,** 1180 (2011).
13. J. Chen, X. Shen, Z. Hong, and X. Li, in *Proceedings of OECC 2010* 8E2-1, (2010).
14. X. Shen, X. Li, L. Zhou, Z. Hong, X. Yu, Y. Zhang, and J. Chen, Chin. Opt. Lett. **9,** 050604 (2011)
15. R. J. Black, S. Lacroix, F. Gonthier, and J. D. Love, IEE Proc. J. **138,** 355 (1991).
16. L. V. Nguyen, D. Hwang, S. Moon, D. S. Moon, and Y. Chung, Opt. Express **16,** 11369 (2008).
17. R. Jha, J. Villatoro, G. Badenes, and V. Pruneri, Opt. Lett. **34**, 617 (2009).
18. E. Li, Opt. Lett. **32,** 2064 (2007).
19. Q. Wu, Y. Semenova, P. Wang, A. M. Hatta, and G. Farrell, Meas. Sci. Technol. **22,** 025203 (2011).